PLASTIC DEFORMATION OF SINGLE CRYSTALS OF SAPPHIRE: BASAL SLIP AND TWINNING*

M. L. KRONBERG†

Structural background has been presented in the form of a model based on a framework of oxide ions in hexagonal closest packing, with aluminum ions in octahedral interstices. Dislocation concepts have then been used for interpreting the significance of the crystallographic elements of slip: $\langle 11\bar{2}0\rangle$, $\{0001\}$, and comparisons have been made with the structurally related hexagonal metals. The Burgers vector of a total dislocation has been discussed in terms of the structure of the crystal, and reasons have been given for questioning whether slip occurs by a total dislocation mechanism. Alternative extended dislocation models have been deduced; the simplest one is based on quarter partials with Burgers vectors identical to those for half partials in the hexagonal metals. In order to move, the quarter partials in question require co-operative displacements of the two kinds of ions. Accordingly, self-pinning occurs if either kind of ion is unable to move.

In addition, it has been shown that the experimentally observed crystallographic elements of deformation twinning can be fully understood only if one assumes that the twinning shears correspond to the synchronized displacements of a quarter partial. Moreover, the classically predicted structure of the twinning interface cannot be achieved by any shear mechanism which also satisfies the experimentally observed shear. On the other hand, the synchronized shear model leads to a classically unpredicted but nevertheless entirely satisfactory kind of twinning interface, which contains a glide plane rather than a true mirror. Consequently, the twinned crystal possesses only a macroscopic mirror plane of symmetry.

The concept of partial slips involving synchronized shears of both kinds of ions should be useful in understanding plastic flow in ionic crystals in general.

DÉFORMATION PLASTIQUE DE MONOCRISTAUX DE SAPHIR: GLISSEMENT BASAL ET MACLAGE

La structure est représentée sous la forme d'un modèle basé sur une ossature hexagonale compacte d'ions oxyde, avec des ions aluminium dans les interstices octahédriques.

La théorie des dislocations a été alors utilisée pour interpréter la signification des éléments cristallographiques du glissement: $\langle 11\bar{2}0\rangle$, $\{0001\}$, et des comparaisons ont été effectuées avec des métaux hexagonaux présentant une structure analogue.

Le vecteur de Burgers d'une dislocation entière est mis en relation avec la structure du cristal et l'on discute le point de savoir si le glissement se fait par un mécanisme de dislocations entières. Des modèles variés de dislocations multiples ont été déduits: le plus simple est basé sur des dislocations partielles dont les vecteurs de Burgers sont identiques à ceux des demi-dislocations partielles dans les métaux hexagonaux.

Pour se mouvoir, les dislocations partielles en question nécessitent des déplacements simultanés de deux sortes d'ions. En conséquence, un bloquage apparait si une des deux sortes d'ions ne peut pas se mouvoir.

De plus, il a été démontré que les éléments cristallographiques de la déformation par maclage observés expérimentalement, peuvent être complètement élucidés dans le cas où l'on suppose que les cissaillements de mâcles correspondent aux déplacements synchronisés des dislocations partielles.

En outre, la structure classique prévue, de l'interface du maclage, ne peut être obtenue par un mécanisme de cisaillement en accord avec celui observé expérimentalement. D'autre part, le modèle de cisaillement synchronisé conduit à une sorte d'interface de maclage classique, non prévue mais cependant totalement satisfaisante.

La conception de glissements partiels entrainant des cisaillements synchronisés des deux sortes d'ions pourrait être utile pour la compréhension de la déformation plastique dans les cristaux ioniques.

PLASTISCHE VERFORMUNG VON SAPHIR-EINKRISTALLEN: BASISGLEITUNG UND ZWILLINGSBILDUNG

Als Ausgangspunkt der Untersuchungen werden die strukturellen Verhältnisse an Hand eines Modells erörtert, wonach die Sauerstoffionen ein Grundgitter mit hexagonal dichtester Packung bilden, in dessen Oktaederlücken die Aluminiumionen eingebaut sind. Sodann werden versetzungstheoretische Gesichtspunkte zur Interpretation der kristallographischen Gleitelemente $\langle 11\bar{2}0\rangle$, $\{0001\}$ herangezogen und Vergleiche mit den strukturell verwandten hexagonalen Metallen angestellt. An Hand der Kristallstruktur wird die Frage des Burgers-Vektors vollständiger Versetzungen erörtert und eine Reihe von Argumenten angegeben, die es fraglich erscheinen lassen, ob das Gleiten mit Hilfe von vollständigen Versetzungen erfolgt. Als Alternative werden Modelle, die mit aufgespaltenen Versetzungen arbeiten, beschrieben. Das einfachste dieser Modelle beruht auf Viertelversetzungen, deren Burgers-Vektor

* Received December 26, 1956.

† General Electric Research Laboratory, Schenectady, New York

identisch ist mit demjenigen der Halbversetzungen in hexagonalen Metallen. Zur Bewegung dieser Viertelversetzungen sind gekoppelte Verrückungen beider Ionenarten erforderlich. Daher tritt eine Selbstverankerung auf, wenn eine Ionenart unbeweglich ist.

Fernerhin wird gezeigt, dass die bei der mechanischen Zwillingsbildung experimentell beobachteten kristallographischen Zwillingselemente nur dann vollständig zu verstehen sind, wenn man annimmt, dass die auftretende Scherung den synchronisierten Verrückungen bei der Bewegung einer Viertelversetzung entspricht. Die mit klassischen Vorstellungen vorausgesagte Struktur der Zwillingsgrenze kann mit keinem Schermechnismus zustande gebracht werden, der mit der experimentell beobachteten Gitterscherung verträglich ist. Das Modell einer synchronisierten Scherung führt auf eine klassisch nicht vorhergesagte, aber trotzdem vollkommen zufriedenstellende Zwillingsgrenze.

Der Vorschlag von Teilversetzungen mit synchronisierter Scherung beider Ionenarten sollte auch für das Verständnis der plastischen Verformung von Ionenkristallen im allgemeinen von Nutzen sein.

1. INTRODUCTION

Recent studies have shown that sapphire (Al_2O_3) and zinc single crystals can undergo plastic basal bending and subsequent polygonization by closely related dislocation mechanisms.[1,2] In this report we shall present the results of an investigation of the slip process in sapphire from the point of view of the crystallography and structure of the crystal as well as the character of the dislocations determined by the structure. Comparisons will be made with the structurally related hexagonal metals. In addition, the results will be used for a structural interpretation of the experimentally determined crystallographic elements of plastic basal twinning.[3]

In essence, the underlying reason for the similarity between the mechanisms of slip and polygonization in the two types of crystals is simply that each is based on a hexagonal closest packing of atoms. It has long been known that crystals of sapphire have oxide ions very nearly in hexagonal closest packing with aluminum ions tucked into the octahedral interstices of the oxygen framework.[4,5] On the other hand, a complete and explicit description of the packing features is not available in the literature. Thus, we shall first describe the detailed structure from a packing point of view.

2. STRUCTURAL BACKGROUND

It is helpful to consider an idealized model based on a perfect packing of spheres, and then to point out the small deviations existing in the real structure.*

The number of octahedral interstices in a hexagonal closest packed structure or framework is equal to the number of spheres which define the framework. Fig. 1(a) shows that the interstices lie on planes midway between contiguous closest packed planes of the framework, and that the positions within such a plane define a simple hexagonal mesh. Part (b) of the figure then illustrates the normal distribution of aluminum ions on the mesh, and furthermore shows that the arrangement of filled and empty interstices is an ordered one.

We shall now show that in three dimensions the positions of the interstices determine a simple hexagonal lattice. The third layer of a hexagonal closest packed framework lies directly above the first (visualize with the aid of Fig. 1a). Accordingly, the octahedral interstices between the second and third layers must be directly above those between the first and second layers. By the same token, all of the hexagonal meshes of interstices must be directly above or below one another. Or in other words, the interstices must lie on the points of a simple hexagonal lattice.

Fig. 2 then shows the normal distribution of cations on this simple lattice. Two-thirds of the octahedral interstices are seen to be occupied, and one-third remain vacant.†

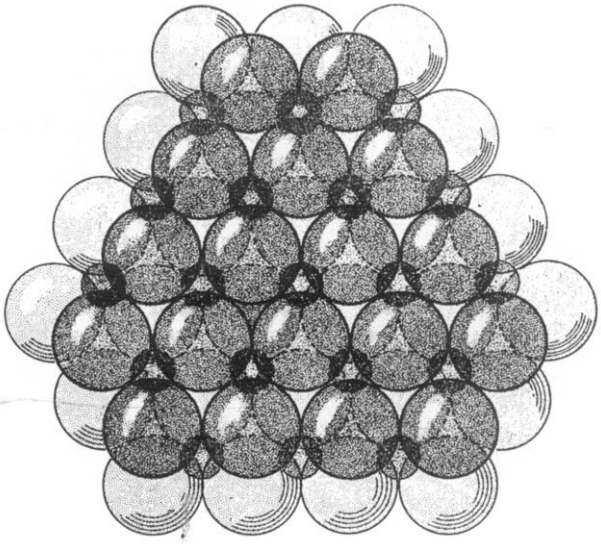

FIG. 1(a). A view normal to two layers of a closest packed structure, showing the positions and relative sizes of the octahedral interstices.

* The reader is referred to Appendix A for the conventional formal specifications of the crystal structure. The model to be described in this report has been developed with the use of these specifications.

† In this report a vacant or unoccupied octahedral interstice in the stoichiometric structure will be called a hole.

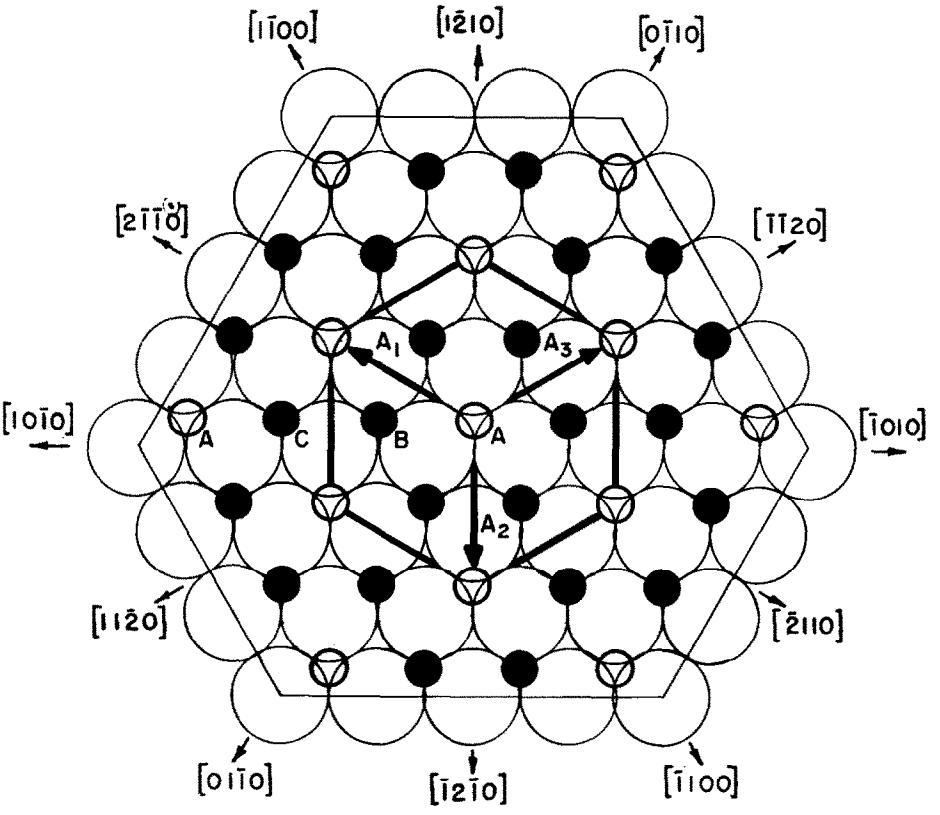

FIG. 1(b). Arrangement of aluminum ions and holes between two layers of oxide ions. Large open circles represent underlying oxide ions, small open circles represent holes, and small filled circles represent aluminum ions. The upper layer of oxide ions is not shown. Basal hexagonal cell vectors and directions are shown.

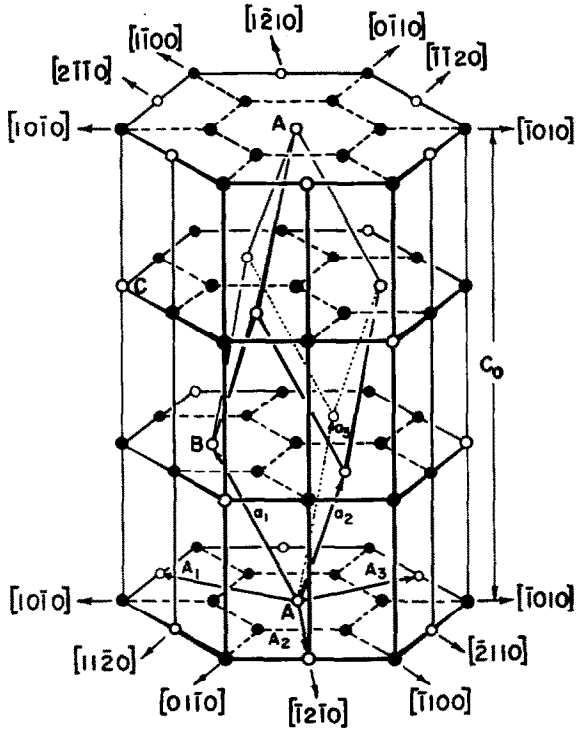

FIG. 2. Distribution of aluminum ions and holes on the simple hexagonal lattice. The smallest rhombohedral cell which correctly describes the positions of the cations is shown along with the corresponding hexagonal cell vectors.

In a formal sense, a hole is a region of localized negative charge, for it is bounded solely by outer electrons of the surrounding oxide ions. Thus the aluminum ions and holes are arranged within the framework so as to give a maximum separation of like charges and a minimum separation of unlike charges, consistent of course with the necessary bonding between oxygen and aluminum and the maintenance of gross electrical neutrality.

For present purposes it is quite useful to describe the lattice of the gross structure in terms of the positions of the holes.* Figs. 1(b) and 2 show the unit hexagonal lattice vectors in the base plane, and the latter shows in addition the C axis of the smallest hexagonal cell which correctly describes the positions of the cations alone.†

It is pertinent to note [Fig. 1(b)] that the ordered positions of the holes define a hexagonal mesh which is a multiple of the corresponding one determined by the oxide ions. In addition, the two meshes differ in orientation by a rotation of 30° about the mesh

* In Pauling's original determination, the origin of coordinates was not a hole. Rather, it was a point along the hexagonal axis of our simple hexagonal cell, midway between a pair of aluminum ions.

† The reader is referred to the appendices for additional crystallographic description.

normals. Consequently, the directions of closest packing of oxide ions have the indices $\langle 10\bar{1}0\rangle$, whereas in a hexagonal metal the closest packed directions are of the form $\langle 11\bar{2}0\rangle$. Similarly, the $\langle 10\bar{1}0\rangle$ directions of the metallic structure become $\langle 11\bar{2}0\rangle$ in the sapphire structure.

Although the mesh arrangement of aluminum ions and holes between every pair of oxide layers is identical, the individual meshes are translated with respect to each other along lines which are parallel to the closest packed directions of the framework. The magnitude of the translation, in going from layer to layer, is always one oxygen-oxygen contact distance. Note that the translation can be described in terms of any one of the three equivalent directions $[10\bar{1}0]$, $[0\bar{1}10]$, and $[\bar{1}100]$, but not in the reverse ones. This condition holds only if the bottom layer is held stationary, and upper layers are then translated. Such a convention will be used throughout the paper.

Thus, if the position in any arbitrary layer be designated by the letter A [see Figs. 1(b) and 2] then the hole is shifted to site B in the layer above, thence to site C in the third layer and back to site A in the fourth layer. In fact, it is convenient to describe the entire structure with this formalized kind of shorthand notation.

Let us represent the positions of the oxygen layers by the numbers 1 and 3, and the octahedral interstitial positions by the number 2. Accordingly, the positions of the holes will be given by the symbols $2A$, $2B$, and $2C$. The appropriate sequence describing the gross structure is given in Fig. 3. One sees that the structural hexagonal C_0 repeat distance is determined by six layers of oxygens with six intervening sheets of aluminums and holes. (See Appendix C.)

The deviations giving rise to the real structure are apparently related to electrostatic interactions between the charges in the structure. For a perfect packing of spheres the packing ratio would be 1.63; whereas in the real structure this ratio is 1.58. Evidently, the attractive forces between the aluminum and oxygen ions are sufficiently strong to pull the oxygen layers closer together than would be the case for perfect packing, despite the fact that the like charged oxide ions are in contact.

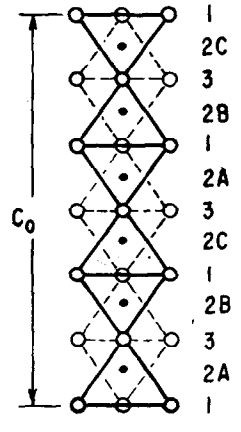

FIG. 3 Projection view along $[\bar{1}2\bar{1}0]$. Open circles represent oxide ions and filled ones designate octahedral sites. C_0 for the structural cell is shown. A shorthand notation is given for the packing.

Expressed in terms of the structural rhombohedral unit cell (see the Appendices), the rhombohedral angle would be 53°47′ for perfect packing; whereas the observed angle is 55°17′.

In the idealized structure the distance between nearest aluminum ions lying on lines parallel to C_0 (Fig. 2) is approximately 18 per cent shorter than the corresponding distance normal to C_0. In the real structure, the two distances become nearly equal by having the former pairs of ions move apart along C_0 toward neighboring holes. As a consequence, the aluminum ions lying in basal planes in the ideal structure become non-coplanar in the real structure, although the oxide sheets remain flat.

The idealized model will be assumed for this report, but attention will be called to the real structure on occasions when it is believed that the deviations have particular significance for the specific matter at hand.

3. PLASTIC DEFORMATION

3.1. *The Slip Process*

3.1.1. *Crystallographic and structural elements*

Single crystals have been observed to slip on basal planes—{0001}. The observation was first made on cylindrical samples having these planes at angles of 30° to 75° to the cylinder axis.[6] The rods could be bent at temperatures as low as 1300°–1400°C, provided the axis of bending was normal to the hexagonal axis.

Wachtman subsequently found that similar samples would creep by basal slip under static tensile loading, at temperatures as low as approximately 900°C at resolved shear stresses of the order of 10,000 lb per sq. in.[7] Tests at 1000°C on samples having the basal planes parallel to the rod axis showed that creep could not be induced for this special orientation.*

From studies of orientation changes in his tensile creep specimens, Wachtman determined the slip direction at 1300°C to be $\langle 11\bar{2}0\rangle$.

Both the slip plane and direction have been confirmed by the author for dynamical tensile loading in the temperature range of 1300°–2000°C.†

* At the time of this writing, Wachtman has informed the author that deformation has been observed at higher temperatures, but that a successful analysis of the crystallographic features had not been accomplished.

† The experiments will be described in a separate paper on dynamical flow properties.

Thus, for the orientations studied, the observed crystallographic elements of slip, $\{0001\}\ \langle 11\bar{2}0\rangle$, are identical with those for a hexagonal crystal like zinc. In a strictly formal sense, the slip process for each type of crystal can be considered to involve an effective net translation of contiguous closest packed basal sheets. For the metallic crystal the plane in question simply shears over an underlying one. On the other hand, for the oxide crystal the shearing plane moves over the intervening interstitial ions as well.

Although the slip directions are identical in a crystallographic sense, i.e. net flow is parallel to the vector which correctly describes the smallest structural repeat translation, it is important to note that they are quite different in a structural sense. For zinc a $\langle 11\bar{2}0\rangle$ direction is parallel to a closest packed row of atoms, but in sapphire a $\langle 11\bar{2}0\rangle$ direction is at 30° to a row of closest packed oxygens. Formal comparisons of the slip directions are made in Fig. 4.

It is significant to recall that all previous studies of slip directions in crystals containing directions of closest packing have shown that flow is always in the direction of closest packing, regardless of whether the crystal be metallic or nonmetallic. Some examples are the various metals, the alkali halides, the silver halides, and magnesium oxide.[8,9] The same is true of the triclinic crystal kyanite, $Al_2O_3 \cdot SiO_2$.[10]

Thus, in a structural sense alone, the observed slip direction in sapphire is decidely anomalous. On the other hand, when interpreted from the point of view of dislocation theory, the anomaly disappears readily. In fact, as we shall see, dislocation theory implicitly predicts the experimentally observed direction. *

3.1.2. *Dislocations*

Total dislocations. According to dislocation theory, the self-energy of a dislocation is proportional to the square of its Burgers vector, B.[11,12] Thus for any given plane, slip should be in the direction of the Burgers vector of that total dislocation which has the shortest possible Burgers vector. Since the Burgers vector of a total dislocation must correspond to a structural repeat translation, one can conclude that slip on the base plane of a hexagonal closest packed crystal should always be along A_0, as is observed for both zinc and sapphire.

Fig. 5 shows the Burgers vectors of the total dislocations for hypothetical flow along $\langle 11\bar{2}0\rangle$ and $\langle 10\bar{1}0\rangle$ directions, respectively. For $\langle 11\bar{2}0\rangle$, $B = A_0$, and for $\langle 10\bar{1}0\rangle$, $B = \sqrt{3}A_0$. Thus, on the basis of the B^2 criterion for self-energy, a total dislocation for flow along $\langle 11\bar{2}0\rangle$ should be favored by a factor of 3 over one for flow along a direction of close packing.

For the case of each of the other crystals referred to earlier as ones which flow along directions of close packing, the shortest structural repeat distance for the particular planes involved is in every case parallel to a close-packed direction. Thus, we see that all the

* The slip direction was correctly predicted prior to experimental determination by J. C. Fisher, E. W. Hart, and the author during joint discussions of the nature of the structure.

FIG. 4. Formal comparison of $\langle 11\bar{2}0\rangle$ slip directions in zinc and sapphire.

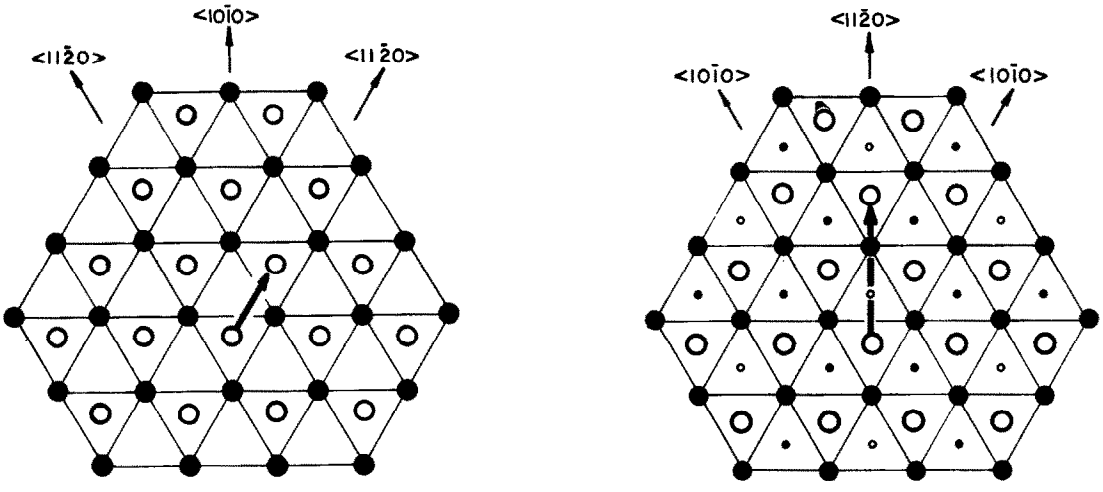

(a) Filled circles represent zinc atoms in an underlying basal plane and open circles represent the atoms in the plane above. The vector describes the smallest displacement that each atom in a given plane must undergo in order to restore the normal structure. It is equal to A_0.

(b) Large filled circles represent oxide ions in an underlying basal plane and large open circles represent oxide ions in the plane above. Small filled and open circles designate aluminum ions and holes, respectively, lying on the median plane between the oxide sheets. The vector has the same significance as for part (a) of the figure.

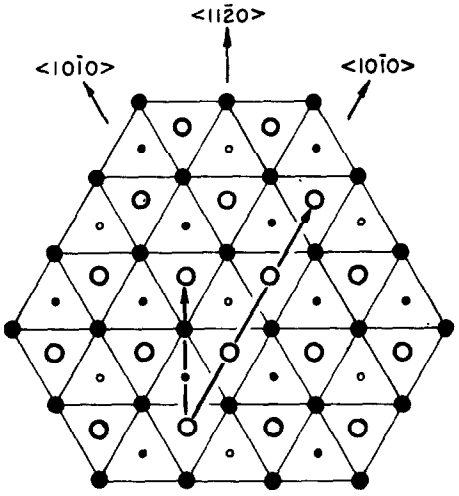

FIG. 5. Comparison of the Burgers vectors for total dislocations for slip in $\langle 11\bar{2}0\rangle$ and $\langle 10\bar{1}0\rangle$ directions.

close-packed crystals studied thus far have slip directions in accord with the B^2 criterion.

Extended dislocations. A total dislocation lying in a close-packed plane can lower its energy by dissociating into an extended dislocation composed of partials (with Burgers vectors shorter than that of the parent total dislocation) separated by ribbons of faulted structure.[11,12] Dissociation will occur only if the energy gained by going to the shorter Burgers vectors is not overbalanced by the increase in energy of the faulted strip in comparison with the normal structure and/or an excessive increase in the strain energies of the partial dislocations.

In considering the subject of dislocation dissociation in sapphire, we shall adopt the useful procedure of considering the dislocations first in terms of the oxide framework alone. Then, at a later stage, attention will be devoted to the interstitial cations.

The question of whether a total dislocation in sapphire can dissociate is a particularly interesting and important one. There are several reasons for asking the question. In the first place, the Burgers vector of the total dislocation is considerably greater than those of several kinds of partials that are readily suggested simply by the nature of the structure. In the second place, it is known that dissociation does in fact occur in the structurally related close-packed metals. Moreover, examination of the path defined by the total slip (or Burgers) vector shows that the total dislocation in motion must cause the moving oxygens of any given layer to climb directly over those below and thus disrupt the close-packed character of the structure (see Figs. 1 and 4). Likewise, such climbing should be unfavorable because of the like charges on the oxide ions.

We shall consider first the partials alone, and then at a later stage the faulted structures associated with the corresponding extended dislocations.

3.1.3. *Dissociation*

Half and quarter partials. The nature of the structure suggests two kinds of hypothetical dissociation. As shown in Fig. 6, a first splitting can be accomplished formally by choosing pairs of half partials with $B = 1/3\ \langle 10\bar{1}0\rangle = A_0/\sqrt{3}$. Since this vector corresponds to a single oxygen-oxygen distance in a direction of closest packing, we recognize that it is identical with the Burgers vector of a total dislocation in a close-packed metal. Obviously, therefore, the second kind of splitting that is suggested is simply additional subdivision of each of these partials, as done for a total dislocation in zinc, to give a resultant of four quarter partials with $B = 1/3\ \langle 11\bar{2}0\rangle = 1/3A_0$ (Fig. 6).

Accordingly, we reach the interesting conclusion that for both zinc and sapphire, the same kinds of partials can be used as components for achieving the specific net flow directions for each crystal. The distinguishing feature for the two types of structures is simply the number of component partials and the manner of combining them.

From an energy standpoint, each quarter partial would have but one-ninth the self-energy of the total dislocation on the basis of the B^2 criterion alone. In addition, there would be the additional decrease in strain energy associated with the elimination of the climbing of oxide ion over oxide ion, as required for the total dislocation.

Synchro-shear partials. Fig. 7 shows the positions of a group of oxide ions before and after the hypothetical

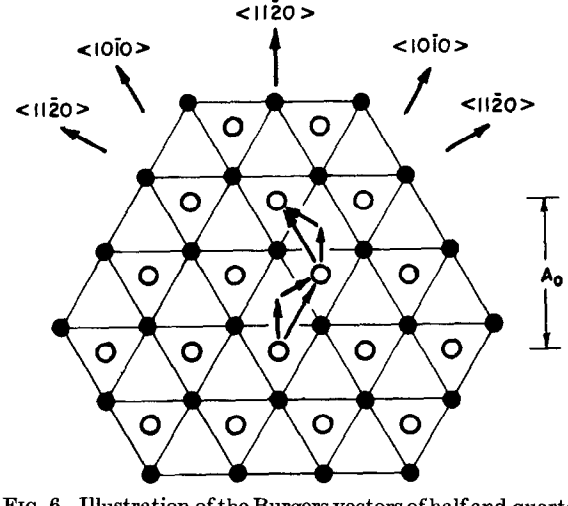

FIG. 6. Illustration of the Burgers vectors of half and quarter partials for component displacements along $\langle 10\bar{1}0\rangle$ and $\langle 11\bar{2}0\rangle$ directions, respectively, of the framework.

passage of a quarter partial, and in addition shows the corresponding relocation of an octahedral interstice. Thus, if an aluminum ion is to have its normal octahedral co-ordination after partial slip of the oxide ions, it must move in a $[2\bar{1}\bar{1}0]$ direction across the saddle determined by atoms 2 and 3 in synchronism with a $[1\bar{2}10]$ displacement of atom 7 across the saddle defined by atoms 1 and 2.

The structure of a partial dislocation which accomplishes the synchronized displacements is shown schematically in Fig. 8. For the sake of simplicity, the construction has been made on the assumption that the shear stress is accommodated entirely on the upper moving plane. This condition is in accordance with the formalized displacements shown in Fig. 7. In any event, the relative positions of the interstitial ions within the framework dislocation would be essentially unchanged by other arbitrary ways of accommodating the stress, for example by resolving it equally on both planes of the framework.

The orientation of the dislocation is shown as being pure screw, for this orientation best shows the co-operative movements of the two kinds of ions. On the other hand, for the general case there is no restriction on the possible orientation in the sense that it can range from pure screw to pure edge. Regardless of orientation, the co-operative movements of both types of ions would be of the kind shown in Fig. 8.

The continuous change in structure across the line of the dislocation can be seen readily with the aid of the figure. Note that the numbered atoms at the bottom of the figure have the "before" positions of Fig. 7, and that the numbers at the top designate the "after" positions. Thus, if we imagine that the individual interstitial positions along the length of the figure represent successive locations of a single aluminum ion A with respect to its environment of oxygens, we see that the cation always remains in direct contact with atoms 2 and 3 as well as 7 and 8. Or in other words, the aluminum ion effectively flows over the underlying saddle of atoms 2 and 3 as the upper identical saddle of atoms 7 and 8 flows over it.

The original octahedral configuration gradually becomes distorted, and the interstitial ion concomitantly loses contact with atoms 1 and 6 of the original octahedron. As it leaves these atoms behind, however, it concurrently approaches atoms 4 and 9, as shown at the halfway point, and then gradually reforms a new octahedron. At the halfway point the original octahedral interstice is no longer recognizable. Rather, the aluminum ion is in fourfold first-neighbor co-ordination, at the center of a transition interstice

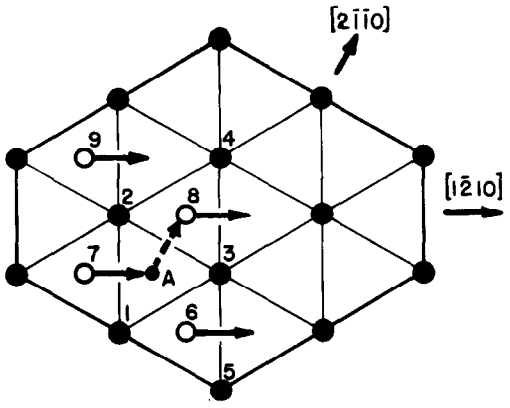

FIG. 7. Representation of the positions of two layers of oxide ions and an intervening octahedral site before and after quarter partial slip. Solid arrows represent the formal displacements of the upper layer, and the dotted arrow leads to the relocated position of the octahedral site.

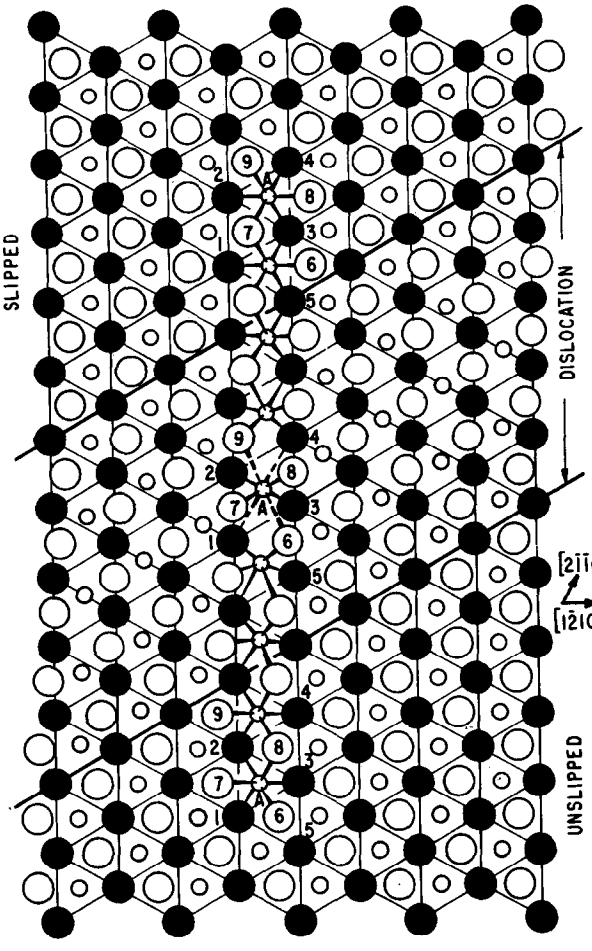

FIG. 8. Illustration of the structure of a quarter partial dislocation, showing both the framework and interstitial positions. The distribution of aluminum ions of the interstitial sites is not shown. It is simply the normal one of Fig. 1(b). Designated positions correspond to those of Fig. 7.

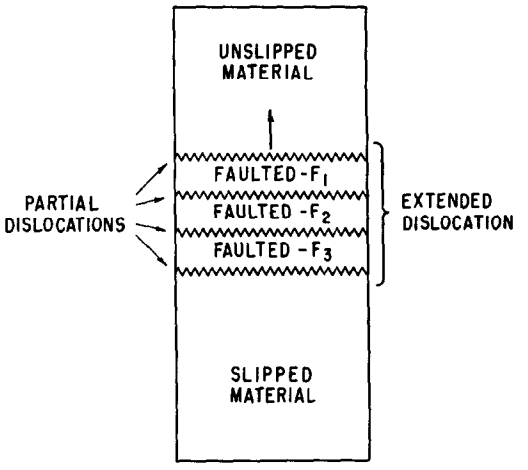

FIG. 9. Schematic representation of an extended dislocation composed of quarter partials separated by strips of faulted structure.

formed by the super-positioning of the two saddle points of the atom pairs 2–3 and 7–8.

It is known experimentally that the Al-O distance for octahedral co-ordination is of the order of 1.90 Å, whereas for tetrahedral it is around 1.70 Å.[13] Simply on the basis of a hard-sphere model, the maximum Al-O distance that could be accommodated in the transition void at the middle of the dislocation is approximately 1.80 Å. Thus, to a first approximation at least, the transition void in question is large enough to pass an aluminum ion, without requiring any dimensional changes in the framework.

An additional and critically significant structural property of the dislocation is that it provides the necessary ionic bonding for holding the oxide sheets in contact with each other. Or in other words, as the dislocation in motion causes the oxide sheets to flow over each other, they are held together by the aluminum

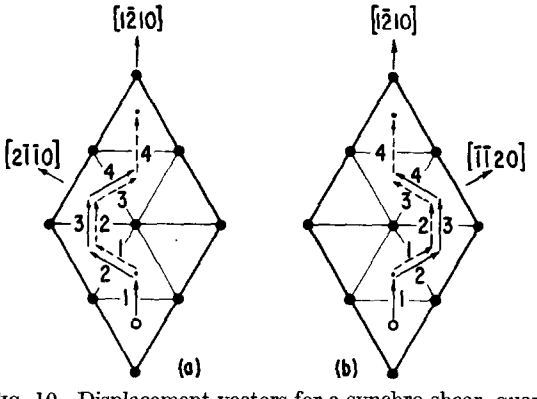

FIG. 10. Displacement vectors for a synchro-shear, quarter partial, extended dislocation. Solid and dashed arrows represent framework and interstitial displacements respectively. Pairs of similarly numbered arrows represent the required pairs of vectors needed to specify each of the four synchro-shears.

ions moving in synchronism through the interstices of the dislocation. It follows, therefore, that the dislocation possesses the inherent property of being self-pinning and thus immobile unless the two kinds of ions are able to move co-operatively with respect to each other.

Since the dislocation causes the framework and interstitial ions to be displaced in different directions, specifically at 120° to each other along a pair of $\langle 11\bar{2}0\rangle$ directions, it cannot be described by a single slip vector as is the case for a hexagonal metal. Slip vectors for both kinds of ions must be specified.

Because of the unusually attractive structural features of the dislocation in question, it now becomes particularly worthwhile to investigate the natures of the faulted structures required for a hypothetical extended dislocation model. For the sake of description, we shall henceforth refer to dislocations involving the discussed synchronized shearing of both kinds of ions as synchro-shear dislocations.*

Faulted structures. Fig. 9 is a schematic illustration of the structure of an extended dislocation based on four quarter partials and three associated faulted structures. A vectorial description for the case of four synchro-shear partials is given in Fig. 10. Two similar but non-equivalent descriptions are shown. Each, however, is based on combinations of displacement vectors of the form 1/3 $\langle 11\bar{2}0\rangle$. The faults encountered along the two routes indicated in the figure will be described for the two cases at hand, starting with the route of part (a).

For the first partial, the sheared portion of the framework is displaced through 1/3 [1$\bar{2}$10] to introduce a conventional stacking fault into the oxygen matrix. Simultaneously the interstitial cations are displaced through 1/3 [2$\bar{1}\bar{1}$0] to occupy octahedral interstices of the faulted framework. The associated change in packing, as well as the arrangement of cations within the altered framework, is shown in Fig. 11.

For the second partial, the sheared portion of the framework is displaced through 1/3 [2$\bar{1}\bar{1}$0], giving a total net displacement thus far of 1/3 [1$\bar{1}$00]. Since the net displacement is equivalent to a single oxygen-oxygen spacing in a direction of closest packing, the stacking fault is therefore removed, and the normal structure of the framework is thus restored. The interstitial ions are concomitantly dispaced through 1/3 [1$\bar{2}$10] to fill octahedral interstices of the normal framework. On the other hand, the interstitials are of

* From the point of view of the formal displacements alone, without regard to mechanism, the synchro-shear model is an outgrowth of the classical congruent shear model of Mathewson.[14] From the dislocation point of view, it is an extension of the partial dislocation model of Heidenreich and Shockley.[15]

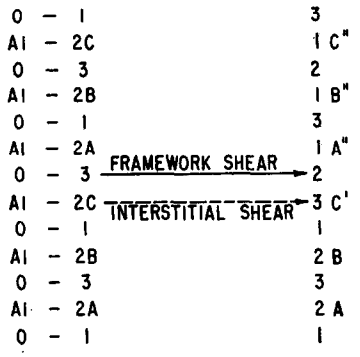

FIG. 11(a). Packing change induced by a synchro-shear of 1/3 [1$\bar{2}$10], 1/3 [2$\bar{1}\bar{1}$0] for the framework and interstitial atoms respectively. The numbers have their usual significance. Singly primed letters refer to the positions of the octahedral holes in the interface and doubly primed ones to the holes in the upper portion of the structure that has been given a bodily displacement of 1/3 [1$\bar{2}$10].

necessity disordered across the shear interface, since the net translation of 1/3 [1$\bar{1}$00] thus far accomplished is not a structural repeat distance. Thus the implied fault is not a stacking fault in the usual sense. Rather, it represents an error in the positive charge distribution within a normal framework. For descriptive purposes we shall therefore call such a disturbed structure an electrostatic fault. For the moment, we shall defer describing the explicit structure of the particular electrostatic fault in question.

The third partial again generates a stacking fault in the framework, similar to the one produced by the first partial. In fact, the over-all faulted structure,

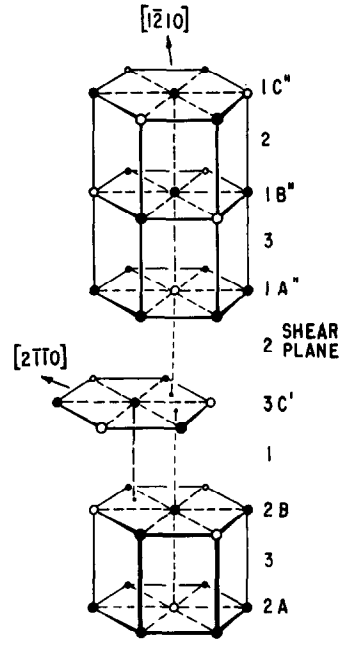

FIG. 11(b). Spatial distribution of cations within the faulted framework. All cations are in octahedral co-ordination.

F_3 is identical with F_1, except that it is rotated 60° about C_0. For present purposes, the rotational reorientation is inconsequential, and we can assume the faults to be identical.

The fourth and final partial then removes the stacking fault and produces completely normal structure that has been slipped through a single A_0 spacing.

An analogous description can be given for the route delineated in Fig. 11(b). The stacking faults are identical with those described, if we ignore the rotational differences in orientation, but a different kind of electrostatic fault is encountered. Fig. 12 then shows the structures of the two electrostatic faults in question.

For route (a) the net displacement leading to the electrostatic fault is 1/3 [1$\bar{1}$00], and for route (b), 1/3 [0$\bar{1}$10]. Note that for the route (a) fault a mirror

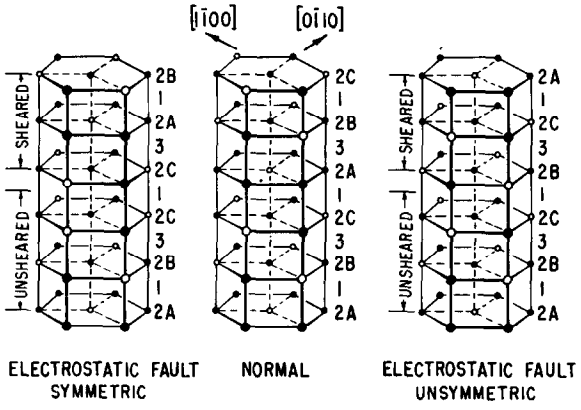

FIG. 12. Electrostatic faults produced by net synchro-shearing through 1/3 [1$\bar{1}$00] and 1/3 [0$\bar{1}$10]. The former shearing produces a symmetric charge distribution across the interface, and the latter an unsymmetric one. Corresponding packing changes are shown.

arrangement of two layers exists across the interface; whereas for the route (b) fault the arrangement is unsymmetrical. For purposes of distinction, we shall therefore call the former fault "symmetric" and the latter one "unsymmetric."

The symmetric configuration represents the poorest possible way of arranging any two arbitrary layers and gives rise to an adverse change in the charge and bond distribution across the interface. In the idealized unsymmetric structure, however, there are no such interfacial deviations; rather the abnormalities are confined to next-nearest neighbors. First-neighbor co-ordination figures for the normal and faulted structures are shown in Fig. 13. The idealized normal structure thus has each oxygen surrounded by four cations and two holes at the corners of a trigonal prism, the holes being located so as to give a maximum

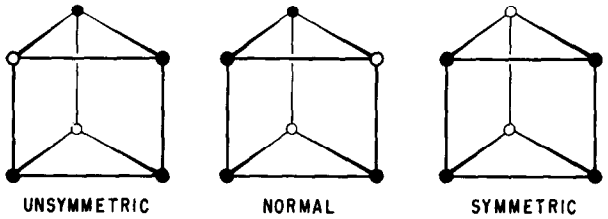

FIG. 13. Trigonal prism co-ordination figures for an oxide ion in the normal and electrostatically faulted structures. The filled and open circles represent the aluminum ions and holes, respectively, surrounding an oxide ion.

separation between them. In the unsymmetric structure an equivalent but permuted distribution prevails; whereas for the symmetric one the holes achieve the closest possible distance of approach. It is reasonable, therefore, to conclude that the unsymmetric fault represents the lesser deviation from normality.

Next-nearest-neighbor deviations in the faulted structures are shown in Fig. 12 in the form of abnormal arrangements along rows parallel to C_0. It will be recalled that in the real structure the pairs of aluminums along C_0 are actually spread approximately 18 per cent from the idealized positions. Accordingly, the strings of three and four, as found in the symmetric and unsymmetric structures respectively, should be successively poorer arrangements. On the other hand, in the unsymmetric structure there is an equal number of adjacent abnormal strings containing alternating cations and holes. Indeed, when considering the real structure, such an arrangement should be ideal for helping relieve the confinement of the members of the contiguous strings of four cations. Normal real separations might at least be simulated closely by separations or combinations of separations, as illustrated for example in Fig. 14. In any event, for present purposes, no further distinction need be made between the two kinds of electrostatic faults.

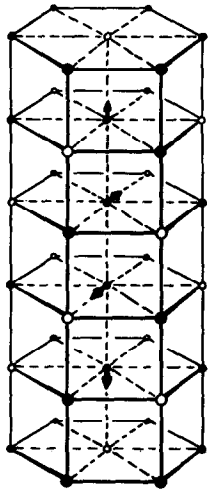

FIG. 14. Displacements for expanding the distances between a string of four aluminum ions in an unsymmetric electrostatically faulted structure.

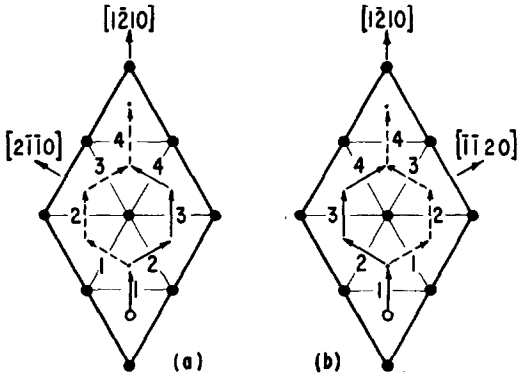

FIG. 15. An alternative combination of displacement vectors for a synchro-shear, quarter partial, extended dislocation. Compare with Fig. 10.

It is true of course that the vector combinations of Fig. 10 are not unique for accomplishing hypothetical net flow along A_0. For example, another pair of combinations is shown in Fig. 15. On the other hand, if the structures of the electrostatic faults associated with these combinations are determined, it will be found that they represent far more serious perturbations than those already discussed. Accordingly, for present purposes any such new combinations will receive no further consideration.

In brief summary, we have deduced a relatively simple extended dislocation model, merely on the basis of determining the shortest Burgers vectors for the partials and the slightest structural alterations for the faults and the dislocations themselves. The best extended model thus involves four synchro-shear partials, two framework stacking faults, and an unsymmetric electrostatic fault.* Although the model appears to be a serious contender in opposition to a total dislocation model, the absence of any direct theoretical or experimental evaluation of the total energies of the two kinds of models rules out any unambiguous choice. In particular, we should like to have more factual knowledge about the relative energies of the faulted structures.

A fruitful area in which to search for such information is the field of deformation twinning, for it is known that twinning dislocations are closely related to partial dislocations, and twin interfaces are closely related to the faults encountered in extended dislocations. Or, looking at the problem in another way, what use can be made of the knowledge thus far

* Similar models can be derived for all of the host of structures based on close packing, regardless of the manner or degree of filling of the octahedral and tetrahedral interstices.

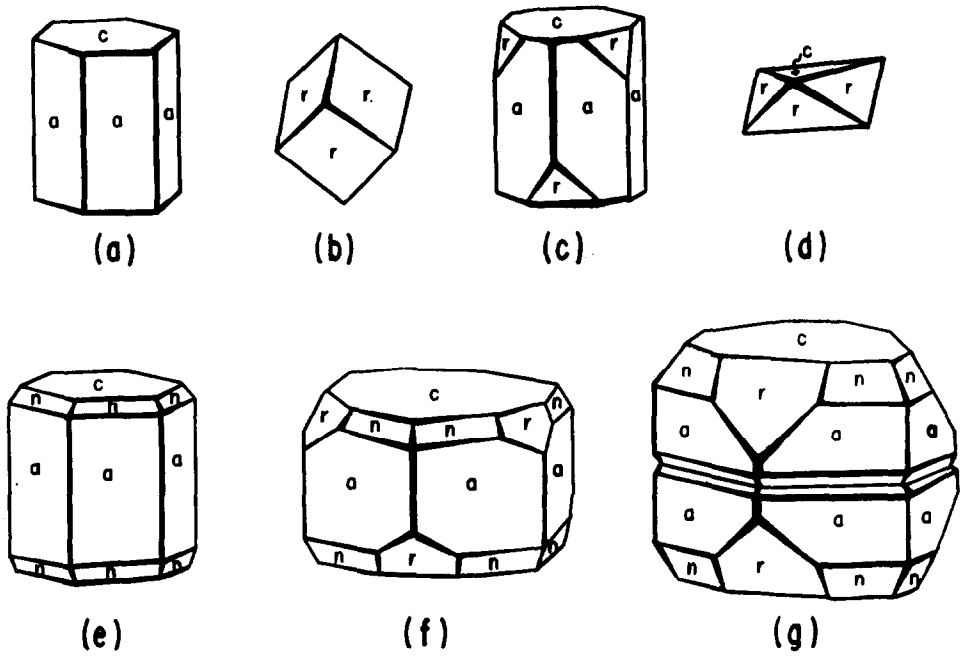

FIG. 16. Drawings of some naturally occurring crystals. All but (g) are normal single crystals. It is a twinned one. Indices of the various faces, in both hexagonal and rhombohedral co-ordinates, are as follows: $C = \{0001\}, \{111\}$; $a = \{11\bar{2}0\}, \{110\}$; $r = \{10\bar{1}1\}, \{100\}$; $n = \{2243\}, \{113\}$. The faces marked "r" are parallel to the faces of the unit morphological rhombohedral cell of Fig. 2.

derived in understanding the mechanism of deformation twinning?

3.2. *Twinning*

3.2.1. *Introduction*

Our current knowledge of basal twinning in sapphire comes exclusively from observations and experiments on natural mineral crystals. Mineralogists have long known that natural sapphire can develop as a basal twin crystal during growth, and moreover that it is possible to induce such twinning by mechanical deformation.[16]

Fig. 16 illustrates the external morphology of some normal and twinned crystals as found in nature.[17] The rhombohedral character is self-evident. Notice in particular that the normal crystal with full facial development, (f), does not have a mirror plane of symmetry parallel to the base plane, but that the twinned crystal, (g), does. The hexagonal close-packed framework of oxygens does of course have a basal plane of symmetry; it is the arrangement of the aluminum ions within the framework which removes this element of symmetry from the total structure.

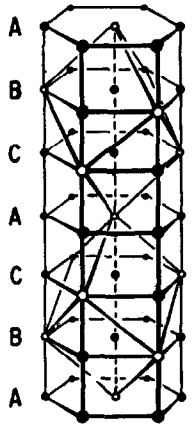

FIG. 17. Hypothetically twinned lattice.

Thus, without disturbing the framework, we can formally construct a twinned structure simply by arranging the holes, i.e. the lattice points, so as to give them a mirror arrangement across a basal lattice plane, as shown in Fig. 17.* Note in particular that the twinning interface is simply an unsymmetric electrostatic type of fault. Quite significantly, the gross structure of the twinned model is in complete accord with the classical rules of lattice twinning.[18,19]

3.2.2. *Crystallographic and structural elements*

Mechanically induced basal twinning has been studied in detail by Veit,[3] utilizing a cylinder and piston mechanism for applying combined hydrostatic and compressive stresses. The procedure consisted of

* A somewhat more elegant representation of the twinned model can be obtained by transforming our co-ordinates back to those of Pauling. So doing would simply be the equivalent of translating our lattice along C_0 until the twin plane of the lattice coincides with the basal symmetry plane of the oxygen framework.

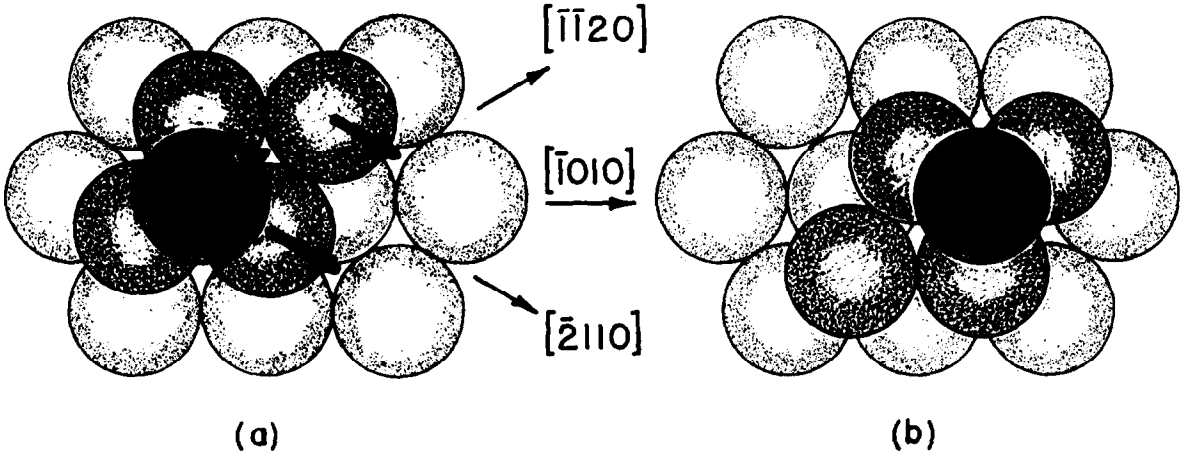

FIG. 18. The component twinning shears for the framework. The bottom layer is held stationary and the upper ones are sheared bodily through 1/3 [$\bar{2}$110]. The third layer is then sheared through 1/3 [$\bar{1}\bar{1}$20].

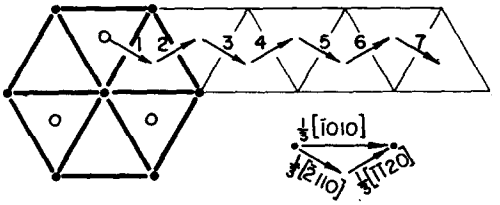

FIG. 19. The sequence of twinning shears for the framework. The successive vectors represent the individual shears of the successive layers above the initial shear interface. The locus of displacements corresponds to the traverse of the macroscopic structure being transported above the zone of shear.

embedding a crystal, with well developed faces, in finely powdered sulfur and then applying pressure in the range of 13,000 to 18,000 atmospheres. After deformation, samples were observed to contain twin lamellae, visible to the naked eye, with well developed crystal faces. From an analysis of the angles between the faces on the deformed and undeformed portions, Veit was able to make a complete and unambiguous determination of the crystallographic elements of twinning. His results are as follows:*

$$K_1 = (0001) = (111) \qquad \sigma_1 = [(0001), (12\bar{1}0)] = [11\bar{2}]$$

$$K_2 = (\bar{2}021) = (\bar{1}11) \qquad \sigma_2 = [(\bar{2}021), (1\bar{2}10)] = [112]$$

$$S = 0.635.$$

In terms of the current structural description, the observed shear direction, σ_1, corresponds to any of the three equivalent directions of closest packing of oxygens: [1$\bar{1}$00], [01$\bar{1}$0], [$\bar{1}$010]. In no case was flow observed for the reverse directions. The magnitude of the shear, S, corresponds formally to a displacement of a single oxygen-oxygen spacing, i.e. 1/3 [1$\bar{1}$00], for every two successive planes that have been sheared.

* Veit has used the conventional hexagonal and rhombohedral indices based on the morphological unit cells. Note that his work was done in 1921 prior to the X-ray diffraction determination of the crystal structure in 1925.

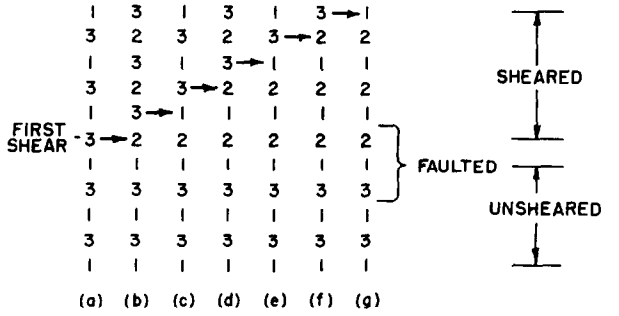

FIG. 20(a) Packing number diagrams showing the changes that would be caused by successive shears of a stack of layers above the original shear interface.

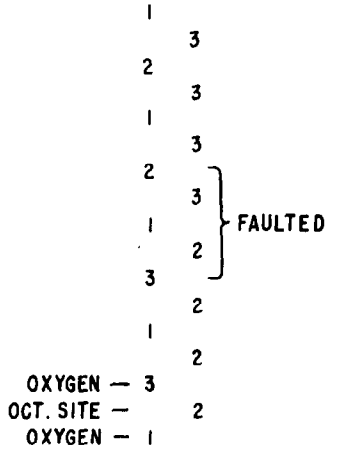

FIG. 20(b) The final configuration of part (a), with the positions of the octahedral voids added. Note that the shearing process interchanges the number 2 and 3 positions.

3.2.3. *Interpretation*

A literal interpretation of the data suggests a flow process based on successive displacements of sandwiched pairs of oxygen sheets (with a layer of cations in the sandwich). On the other hand, such a mechanism cannot possibly generate a twinned structure. Rather, it can only change the crystal structure of the sheared portion. Although the oxygen framework would be normal after deformation, the gross structure would be incorrect because of an abnormal reordering of the sheets of aluminums and holes. This condition would be true regardless of whether one considers the formal shearing process to carry the sandwiched oxygen layers directly over the cations lying in the interface between sandwiches, or to induce them to flow along in unison. Thus, we reach the significant conclusion that the classically predicted twinned structure cannot be achieved by a shearing mechanism which would be in accord with the experimentally observed shear requirements.

On the other hand, an unpredicted but nevertheless entirely satisfactory structure can be derived on the basis of an alternative interpretation of the shear data. Let us assume that *none* of the actual displacements need be in the observed shear direction, $[1\bar{1}00]$, and thus not within the observed plane of shear. Rather, only the *projected* contributions need satisfy the shear requirements. Or in terms of the framework, each oxygen layer need only contribute a flow component whose projection on $[1\bar{1}00]$ is half an oxygen-oxygen spacing.

From our studies of extended dislocations, we readily recognise that half an oxygen-oxygen spacing along $[1\bar{1}00]$ is simply the projected magnitude of the slip (or Burgers) vector of a quarter partial dislocation, $B = 1/3\ \langle 11\bar{2}0\rangle$. Thus, in terms of successive layers of the framework, the shear requirements can be satisfied uniquely if the first layer to be sheared produces a displacement of $1/3\ [\bar{2}110]$, the second layer an additional displacement of $1/3\ [\bar{1}\bar{1}20]$, and so on in sequential repetition. The sequence holds, however, only if the first shear is on a number 3 layer. If the shearing starts on a number 1 layer, then the order of the two component displacements must be inverted. Figs. 18 and 19 illustrate the operations for the former case.

The packing alterations induced in the framework by such a sequence of shears are illustrated in Fig. 20(a). The sheared and unsheared portions are each in normal hexagonal packing but are not in mirror imagery. Rather, the gross framework simply contains a stacking fault at the shear interface. In fact, the central five layers are in double hexagonal closest packing, which is the normal arrangement of oxygens in brookite (TiO_2) and topaz ($Al_2F_2SiO_4$).[13]

Study of the figure shows that the oxygen layers maintain a number 1 packing position throughout, but the number 3 type of layer has moved into position 2 in the sheared portion. In other words, the number 3 oxygen positions and the number 2 octahedral site positions have simply interchanged, as shown in Fig. 20(b) of the figure.

Because of the hexagonal symmetry of the framework, it is of course possible to develop the sheared configuration for the framework alone by net translations in either direction of a close-packed row. Consideration, however, of the associated synchro-shear displacements of the aluminum ions provides an unambiguous answer to why the observed direction only can be achieved experimentally. At the same time, we shall see how the concomitantly reordered positions of the holes (the lattice points) converts the faulted framework into a satisfactorily twinned structure.

Fig. 21 shows the total traverses of each of the successive layers of the sheared framework for net flow along both senses of a $\langle 10\bar{1}0\rangle$ direction, and at the same time indicates the associated traverses of the intervening layers of octahedral interstices.* The latter traverses are then shown in Fig. 22 for the holes alone. Notice that net flow along $[10\bar{1}0]$ would develop strings of holes exclusively along lines parallel to C_0. Such a rearrangement would be completely untenable; accordingly, flow in this direction would not occur experimentally.

However, we see from part (b) of the figure that flow in the observed $[\bar{1}010]$ direction simply regenerates the normal structure. On the other hand, the packing sequence is simultaneously inverted, as shown in detail in Fig. 23. Note in addition, however, that the reconstructed portion of lattice is formally displaced from the undeformed portion by an amount equal to $1/3\ [\bar{1}\bar{1}20]$. As a consequence, the arrangement of aluminum ions and holes at the interface has been altered from the normal prismatic configuration to octahedral. The resulting arrangement is shown in Fig. 24.

Evidently, the shearing process has introduced only a macroscopic plane of symmetry at the shear interface, for there is of necessity a lattice discontinuity across the interface. The two portions are thus related by a glide plane rather than a true mirror,

* As demonstrated in the earlier section on synchro-shear displacements, the interstices do not travel as entities. Strictly speaking, the traverse vectors for the holes really denote the successive positions of the reconstituted holes.

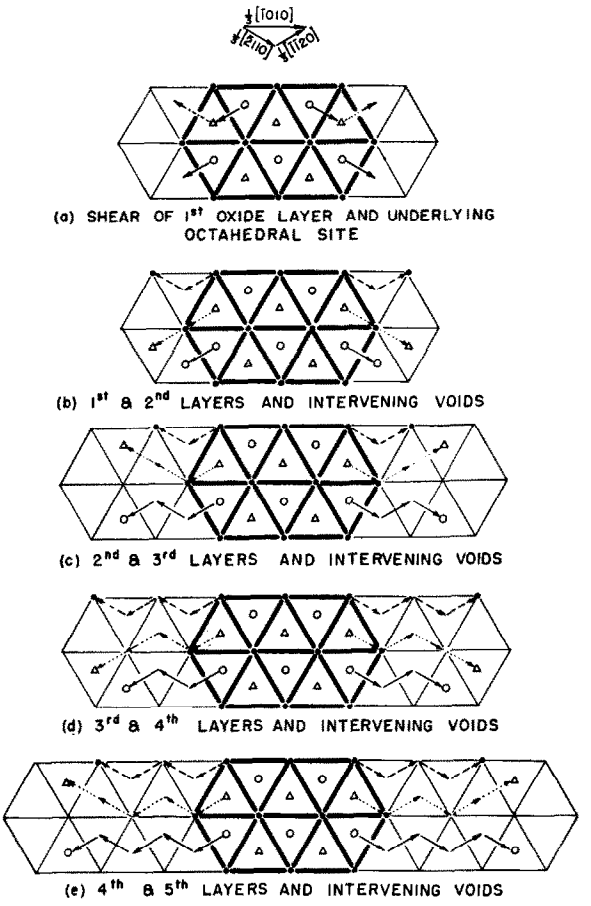

FIG. 21.
(a) Co-operative displacements of a layer of oxide ions and the contiguous octahedral sites below. All layers above undergo a displacement identical to that of the first oxygen translation. Filled circles represent a stationary underlying layer, open circles represent the upper layer to be sheared, and triangles represent the intervening octahedral voids.
(b) Total traverse of first and second sheared oxide layers and intervening octahedral sites. Filled circles represent the second layer to be sheared.
(c) Same for second and third layers and intervening sites. Filled circles represent the second layer to be sheared.
(d) Same for third and fourth layer and intervening sites. Filled circles represent the fourth layer to be sheared.
(e) Same for fourth and fifth layer and intervening sites. Filled circles represent the fourth layer to be sheared.
All displacements prior to the final one for each figure are induced by the preceding shears of underlying layers.

as would be required by the classical lattice rules for twinning. In a formal sense, therefore, the sheared portion is related to the unsheared by a mirror reflection across (0001) plus a translation of 1/3 [$\bar{1}\bar{1}20$].

In terms of the structure, however, both portions are continuously joined; they simply share a faulted segment. Although the shearing process has not produced a twinned crystal which is in accord with the classical lattice rules for twinning, it has nevertheless produced a structure which is in complete accordance with all the experimentally observed requirements.

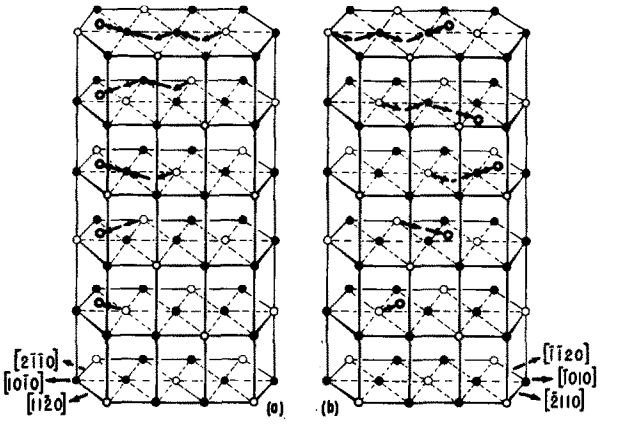

FIG. 22. Total traverses of the holes above the shear interface for the two net directions of flow: (a) [10$\bar{1}$0], (b) [$\bar{1}$010]. (See Fig. 21.)

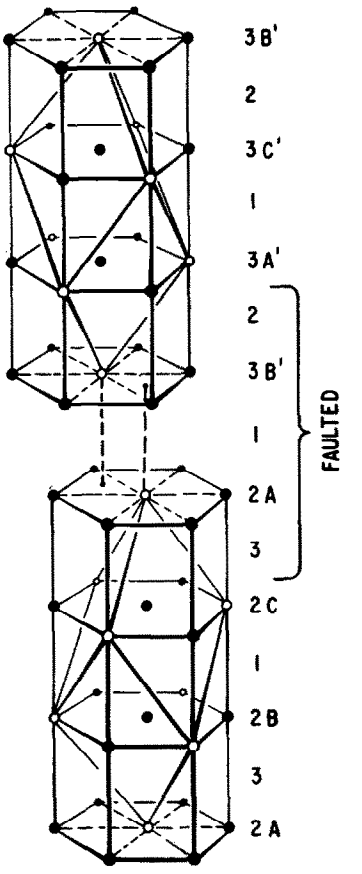

FIG. 23. Lattice reorientation produced by synchro-shearing of successive layers of structure. The upper part has been sheared, and primed letters indicate the relocated position of the holes.

In the absence of any alternative possibilities, the structure in question can be accepted as the correct one for the twinned configuration.*

* In a very comprehensive paper on the general subject of twinning, Cahn[19] has recently reviewed other cases of unconventionally twinned structures.

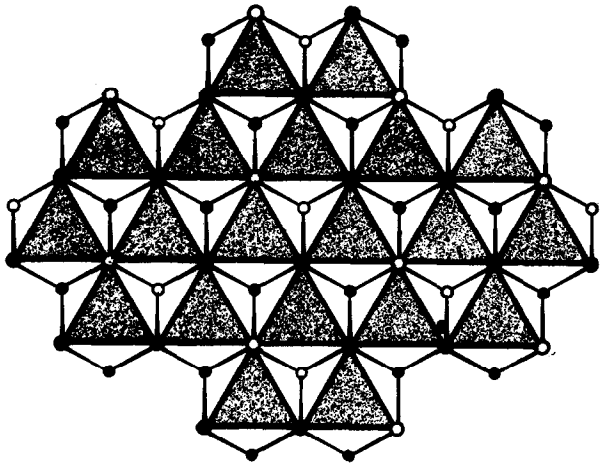

FIG. 24. Octahedral arrangement of aluminum ions and holes surrounding the number 1 oxygens in the interfacial region of the synchro-sheared structure. (See Fig. 23.)

4. DISCUSSION AND IMPLICATIONS

4.1. *Slip*

The success of the synchro-shear model in providing a unique interpretation of the experimental observations on deformation twinning has significant implications regarding the slip process. In the first place, we now have good reason to believe that the co-operative shear, with displacement vectors of the form $1/3\ \langle 11\bar{2}0\rangle$, can occur in real crystals. By the same token, the energy of the stacking fault produced by such a shear must be sufficiently low to allow the fault to be produced by plastic deformation.

Recalling that the synchro-shear extended dislocation model for slip involves two equivalent stacking faults and an electrostatic fault, we see that a remaining unknown is the relative energy of an electrostatic fault. In essence, the latter fault is encountered along the detour part of the extended flow route, which avoids having oxide ions flow directly over each other as would be required by the unit dislocation route. In other words, we must weigh the structural disadvantages of an electrostatic fault against the disadvantages of a disruption of the close packing of the oxide ions. In this light, it is reasonable to hypothesize that the by-pass route should be the preferred one. The argument, however, cannot be pursued further simply with the structural approach used in this report.

4.2. *Twinning*

It is important to realize that the current work on deformation twinning does not discredit the classical structure as being a "bad" one. It shows only that the structure cannot be formed by a mechanism which satisfies the experimentally determined shear requirements. One can readily envisage two hypothetical shearing processes which would lead to the classical structure.

In one case, each layer of oxygen would require a shear of $1/3\ [\bar{1}010]$, and the interstitial aluminum ions below would not move. In the other case, each oxygen layer would have a net shear of $1/3\ [\bar{1}010]$, but would occur by successive displacements of $1/3\ [\bar{2}110]$ and $1/3\ [\bar{1}\bar{1}20]$ for the number 3 layers, and $1/3\ [\bar{1}\bar{1}20]$ and $1/3\ [\bar{2}110]$ for the number 1 layers. The intervening aluminum ions would undergo the required synchro-shear displacements. For each model however, the net shear would be twice the experimental value.

On the other hand, either structure could be generated by a growth process. The classical one could develop by having an error made in the filling of the octahedral interstices; whereas the current one could form by having an error made in the packing of oxygens. The relative probabilities of formation would be related to the currently unknown relative energies of the individual twinning interfaces.

Thus, we conclude that the kinetics of the process leading to twin formation are the critical factors which determine whether any particular twin structure will form. Conventional lattice theory only predicts the formal crystallographic planes that are hypothetically possible for twinning, but does not necessarily predict the structure of the twinning interface.

These conclusions have significant implications in the general field of deformation twinning. Numerous analyses of "atom movements" during twinning have been made on the implicit assumption that lattice theory correctly predicts the structure of a twin.[19,20] For the simplest structures having complete coincidence between lattice points and atomic positions, the assumption is valid. In the general case it is not necessarily so.

Likewise, in the general usage of abstract shear diagram representations of twinning,[19,20] it has been assumed frequently that the atomic displacements leading to twinning lie in the experimentally observed plane of shear. Such a condition is not necessarily so; only the projected flow must satisfy the requirements of the experimentally determined shear specifications.

Accordingly, we reach the conclusion that the conventional shear diagram approach, based on an *a priori* assumption of the structure of the twin, must be used with considerable caution. In particular, adequate attention must be devoted to the nature of the structure itself, and especially the inherent structural properties which either endow it with, or deprive it of, the capacity to react to a stress by flowing along any of its specific crystallographic

planes. The subject will be developed further in separate publications on rhombohedral twinning in sapphire and the various forms of pyramidal twinning in the hexagonal metals.

ACKNOWLEDGMENTS

It is a pleasure for me to acknowledge my indebtedness to J. E. Burke, J. C. Fisher, and E. W. Hart for many discussions during the course of the work, and to J. H. Hollomon, who once showed me a bent sapphire and thus stimulated my initial interest. Mrs. Harriet F. Thackrah deserves much credit for her skillful preparation of the figures.

APPENDIX A

Formal Crystallographic Specifications

Space group: $D_3^6d = R\bar{3}C$

Cell:* Rhombohedral-hexagonal

Lattice parameters:

$a_0 = 5.12$ Å, $\alpha = 55°17'$, $n = 2$ (rhombohedral)

$A_0 = 4.75$ Å, $C_0 = 12.97$ Å, $n = 6$ (hexagonal).

Atomic positions (rhombohedral co-ordinates):

Al: WWW, $\overline{WWW}$, $\frac{1}{2}-W\ \frac{1}{2}-W\ \frac{1}{2}-W$, $W+\frac{1}{2}\ W+\frac{1}{2}\ W+\frac{1}{2}$

O: $u\bar{u}o$, $\bar{u}ou$, $ou\bar{u}$, $\frac{1}{2}-u\ u+\frac{1}{2}\ \frac{1}{2}$, $u+\frac{1}{2}\ \frac{1}{2}\ \frac{1}{2}-u$, $\frac{1}{2}\ \frac{1}{2}-u\ u+\frac{1}{2}$

$$u = 0.303 \pm 0.003$$

$$W = 0.1050 \pm 0.0010$$

APPENDIX B

Rhombohedral and Hexagonal Cell Relationships

Two types of transformation are given below. Figure B-1 shows the relationship between a singly primitive rhombohedral cell and its derivative, the triply primitive hexagonal cell. Figure B-2 shows the relationship for the reverse kind of transformation,

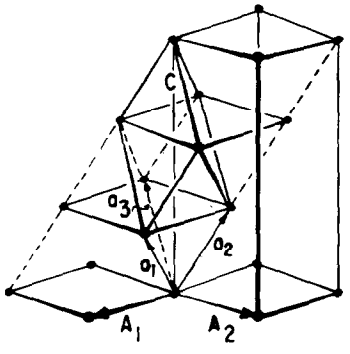

FIG. B-1 Primitive rhombohedral to hexagonal.

* Appendix B describes the relationships between rhombohedral and hexagonal cells.

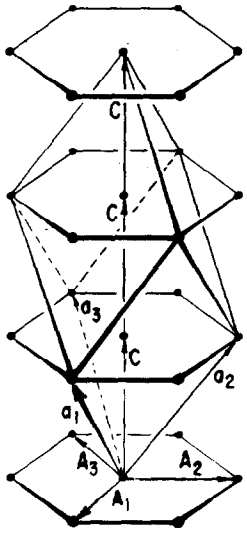

FIG. B-2 Primitive hexagonal to rhombohedral.

namely a singly primitive hexagonal cell to a triply primitive rhombohedral one. Figure B-1 holds for sapphire, whereas Fig. B-2 holds for the hexagonal metals.

APPENDIX C

Morphological and Structural Unit Cells

Prior to the determination of the structures of crystals by the methods of X-ray diffraction, mineralogists had made exhaustive studies of the external morphology of numerous natural minerals. From analyses of the occurrence and absence of specific growth faces they were able to describe the external morphology in terms of unit cells of structure and corresponding crystallographic indices. Of course, absolute values for the magnitudes of the cell vectors could not be determined, but it was possible to evaluate axial ratios as well as the angles between the unit cell vectors.

The relatively recent determinations of the arrangements of atoms within crystals have shown that the morphological cell is either identical with the structural unit cell or is simply related to it. For sapphire there is no identity, but the relationship between the two can be deduced readily.

For the morphological hexagonal unit cell, the C/A ratio has been determined to be 1.365, whereas the value for the true structural cell is 2.730. Thus, if we equate A_0 for the two cells, it follows that the morphological cell is only half as high as the structural one. Or in other words, the morphological C_0 translation is accomplished by three layers of oxygens with three sheets of contiguous aluminums and holes [see Fig. 2 of the text]. Finally, the relationship between the vectors of the various cells is illustrated in Fig. C-1,

and the full rhombohedral cells are shown in Fig. C-2.

As checks on these deductions, the calculated value for the morphological rhombohedral angle, α, corresponds in fact to the observed value of 85°45′.

It is particularly interesting to note that the morphological rhombohedral unit cell is the smallest one which correctly describes the arrangement of the cations alone. On considering both types of ions, however, the larger rhombohedral cell is the smallest one which correctly describes the over-all structure.

Although in a basic sense it might seem that usage of the morphological cells should be abandoned in favor of the structural unit cells, there are compelling reasons for not doing so, at least for studies of mechanical properties. Morphological cells naturally have their surfaces parallel to well-developed growth faces, which in turn are generally defined by atomic surfaces of relatively high atomic density. Since mechanical properties are frequently described in terms of the most densely populated planes, one can readily use the very simple indices and well-known names of the morphological faces without running counter to the terminology and nomenclature of a self-consistent body of literature and thought that is several centuries old.

Although the mineralogists and X-ray crystallographers are currently in conflict over which cell and nomenclature should be used, it would seem that the basic need is not one of distinction (or extinction) but rather of understanding the relationships between

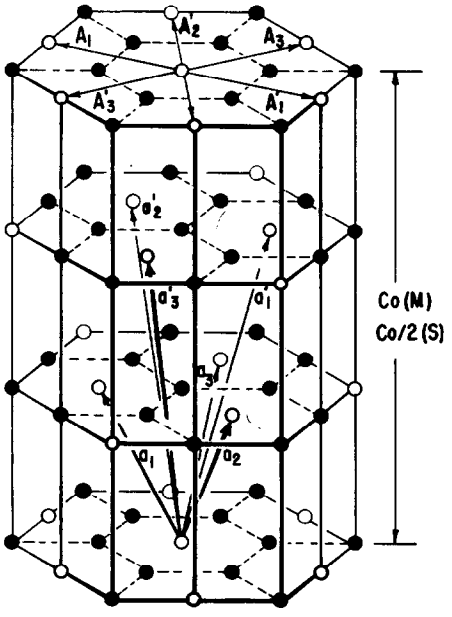

FIG. C–1 Unit cell vectors for the morphological and structural unit cells. Primed letters indicate structural vectors. In hexagonal coordinates, the C_0 vector of the morphological cell is half that of the structural one.

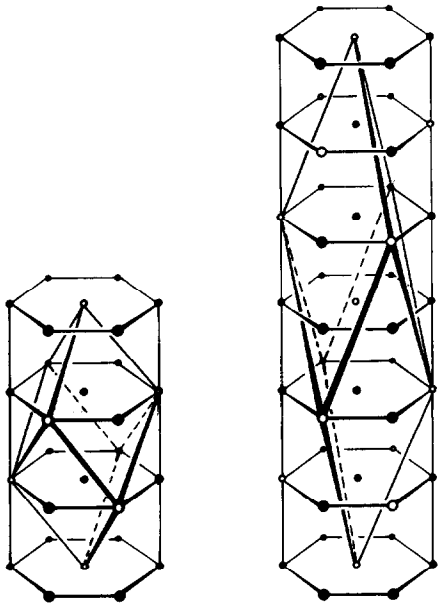

FIG. C–2 The morphological and structural rhombohedral unit cells.

the two kinds of cells. It would then be in order for an investigator to utilize whichever is simpler or more useful for the matter at hand.

For studying those properties of sapphire which are determined by the structure of the basal plane, there is no *a priori* advantage to selecting one cell in preference to the other, since the basal planes are parallel and identical except for the conventions regarding indices. For studies of rhombohedral twinning, however, the morphological cell is much to be preferred.* Accordingly, in these papers the morphological indices will be used as given in Figs. 1(b) and 2 unless specific mention is otherwise made of the structural indices or cell.

REFERENCES

1. J. F. NYE *Acta Met.* **1,** 153 (1953).
2. M. L. KRONBERG *Science* **122,** 599 (1955).
3. K. VEIT *Jb. Min.* Beil, -Bd. **45,** 121 (1921).
4. L. PAULING and S. HENDRICKS *J. Amer. Chem. Soc.* **47,** 781 (1925).
5. W. L. BRAGG *Atomic Structure of Minerals* Cornell Univ. Press (1939).
6. E. L. MCCANDLESS and D. M. YENNI U.S. Pat. 2,485,979 (1949).
7. J. B. WACHTMAN and L. H. MAXWELL *J. Amer. Ceram. Soc.* **37,** 291 (1954).
8. C. S. BARRETT *Structure of Metals* McGraw-Hill, New York (1952).
9. M. J. BUERGER *Amer. Min.* **15,** 1 (1930).
10. O. MÜGGE *Neues Jahrbuch* **II,** 81 (1892).
11. W. T. READ *Dislocations in Crystals* McGraw-Hill, New York (1953).

* Rhombohedral twinning will be the subject of the next report in this series.

12. A. H. COTTRELL *Dislocations and Plastic Flow in Crystals* Oxford University Press (1953).
13. L. PAULING *Nature of the Chemical Bond* Cornell University Press (1940).
14. C. H. MATHEWSON *Trans. Conn. Acad. Arts Sci.* **38,** 213 (1951).
15. R. D. HEIDENREICH and W. SHOCKLEY *Report of a Conference on the Strength of Solids* University of Bristol, England; Physical Society, London, 57 (1948).
16. PALACHE, BERMAN, and FRONDEL *Dana's System of Mineralogy* Vol. 1. John Wiley, New York (1946).
17. V. GOLDSCHMIDT *Atlas der Krystalformen* Band 5 Carl Winters Universital Buchanlung, Heidelberg (1918).
18. G. FRIEDEL *Lecons de Cristallographie* Berger-Levrault (1926).
19. R. W. CAHN *Advances in Physics* **3,** 363 (1954).
20. E. O. HALL *Twinning* Butterworths, London (1954).